Author Manuscript

Author Manuscript

Author Manuscript

Author Manuscript

HHS Public Access

Author manuscript

J Control Release. Author manuscript; available in PMC 2020 March 10.

Published in final edited form as:

J Control Release. 2019 March 10; 297: 3–13. doi:10.1016/j.jconrel.2019.01.036.

Functional Assessment of Peptide-Modified PLGA Nanoparticles against Oral Biofilms in a Murine Model of Periodontitis

Mohamed Y. Mahmoud[d,e,f,1], **Jill M. Steinbach-Rankins**[b,c,d,e,1,*], and **Donald R. Demuth**[a,c,1,**]

[a]Department of Oral Immunology and Infectious Diseases, University of Louisville School of Dentistry, 501 S. Preston St., Louisville. KY, 40202

[b]Department of Bioengineering, University of Louisville Speed School of Engineering

[c]Department of Microbiology and Immunology, University of Louisville School of Medicine

[d]Department of Pharmacology and Toxicology, University of Louisville School of Medicine

[e]Center for Predictive Medicine' University of Louisville, 505 S. Hancock St., Louisville, KY 40202

[f]Department of Toxicology, Forensic Medicine and Veterinary Regulations, Faculty of Veterinary Medicine, Cairo University, Egypt

Abstract

The interaction of the periodontal pathogen *Porphyromonas gingivalis* (*Pg*) with commensal streptococci promotes *Pg* colonization of the oral cavity. Previously, we demonstrated that a peptide (BAR) derived from *Streptococcus gordonii* (*Sg*) potently inhibited adherence of *Pg* to streptococci and reduced *Pg* virulence in a mouse model of periodontitis. Thus, BAR may represent a novel therapeutic to control periodontitis by preventing *Pg* colonization of the oral cavity. However, while BAR inhibited the initial formation of *Pg*/*Sg* biofilms, much higher concentrations of peptide were required to disrupt an established *Pg/Sg* biofilm. To improve the activity of the peptide, poly(lactic-co-glycolic acid) (PLGA) nanoparticles were surface-modified with BAR and shown to more potently disrupt *Pg/Sg* biofilms relative to an equimolar amount of free peptide. The goal of this work was to determine the *in vivo* efficacy of BAR-modified NPs (BNPs) and to assess the toxicity of BNPs against human gingival epithelial cells. *In vivo* efficacy of BNPs was assessed using a murine model of periodontitis by measuring alveolar bone resorption and gingival IL-17 expression as outcomes of *Pg*-induced inflammation. Infection of mice with *Pg* and *Sg* resulted in a significant increase in alveolar bone loss and gingival IL-17 expression over sham-infected animals. Treatment of *Pg/Sg* infected mice with BNPs reduced bone loss and IL-17 expression almost to the levels of sham-infected mice and to a greater extent than treatment with an equimolar amount of free BAR. The cytotoxicity of the maximum concentration of BNPs and free BAR used in *in vitro* and *in vivo* studies (1.3 and 3.4 μM), was

*Correspondence to: Jill M. Steinbach-Rankins, Department of Bioengineering, University of Louisville Speed School of Engineering, 505 S. Hancock St., Room 623, Louisville, KY 40202. **Correspondence to: Donald R. Demuth, Department of Oral Immunology and Infectious Diseases, University of Louisville School of Dentistry, 501 S. Preston St., Room 261, Louisville, KY 40202.
[1]Co-Senior and Corresponding Authors.

Publisher's Disclaimer: This is a PDF file of an unedited manuscript that has been accepted for publication. As a service to our customers we are providing this early version of the manuscript. The manuscript will undergo copyediting, typesetting, and review of the resulting proof before it is published in its final citable form. Please note that during the production process errors may be discovered which could affect the content, and all legal disclaimers that apply to the journal pertain.

Author Manuscript Author Manuscript Author Manuscript Author Manuscript

evaluated in telomerase immortalized gingival keratinocytes (TIGKs) by measuring cell viability, cell lysis and apoptosis. BNPs were also tested for hemolytic activity against sheep erythrocytes. TIGKs treated with BNPs or free BAR demonstrated greater than 90% viability and no significant lysis or apoptosis relative to untreated cells. In addition, neither BNPs nor free BAR exhibited hemolytic activity. In summary, BNPs were non-toxic within the evaluated concentration range of 1.3 – 3.4 μM and provided more efficacious protection against *Pg*-induced inflammation *in vivo*, highlighting the potential of BNPs as a biocompatible platform for translatable oral biofilm applications.

Keywords

Polymer Nanoparticle; Poly(lactic-co-glycolic acid); Peptide Delivery; Drug Delivery; *Porphyromonas gingivalis*; *Streptococcus gordonii*; Periodontal Disease; Oral Biofilm

INTRODUCTION

Periodontal diseases are globally prevalent inflammatory disorders characterized by formation of periodontal pockets, destruction of connective tissue, and alveolar bone resorption leading to early tooth loss. The progression of periodontal disease, if left untreated, can also contribute to systemic conditions of increased cancer risk, cardiovascular disease, diabetes, rheumatoid arthritis, pulmonary disease, and obesity [1, 2]. Of the organisms associated with chronic adult periodontal disease, *Porphyromonas gingivalis* (*Pg*) has been identified as a key pathogen involved in the initiation and progression of periodontal inflammat ion in a murine model of infection. *Pg* is believed to disrupt host-microbe homeostasis and induce populational changes in the subgingival biofilm, driving inflammation, subsequent tissue destruction, and alveolar bone loss [3–6], all of which are primary outcomes in human periodontal diseases [7]. An early step in the colonization of the oral cavity by *Pg* is its adherence to oral streptococci in the supragingival biofilm and this interaction represents an ideal target for therapeutic intervention [1].

The most common and currently employed periodontal treatments consist of physical methods such as scaling and root planing to remove the oral biofilm, followed by antibiotic therapy. However, variation in patient response and the immediate reformation of the oral biofilm post-removal can promote disease recurrence. In addition to the challenges associated with mechanical debridement, the administration of local and systemic antibiotics can enhance opportunistic fungal infections, potential allergic reactions, or the emergence of antibacterial resistant species. Moreover, current antibiotics may non-specifically disrupt microbial homeostasis by killing commensal organisms, and often high, frequently administered doses are required to penetrate periodontal biofilms [8–10]. Given these challenges, the development of more specific agents targeting periodontal pathogens has the potential to offer safer and more effective alternatives against oral biofilms. While several studies have investigated natural and synthetic biologics against oral inflammation and biofilms, including Punica granatum extract [11] *H. madagascariensis* leaf extract [12], miR-146a [13], and the anti-inflammatory agent 15d-PGJ2 [14], our approach has been to

Author Manuscript Author Manuscript Author Manuscript Author Manuscript

target the specific interaction between *Pg* and oral streptococci that contributes to the initial colonization of the oral cavity leading to the development of periodontal disease [15].

Previous work in our group has shown that *Pg* adherence to streptococci is driven by the interaction of the minor fimbrial antigen (Mfa) of *Pg* with streptococcal antigen (e.g., SspB) I/II (AgI/II) [16, 17]. SspB polypeptide is a multifunctional surface protein of *S. gordonii* and is a member of antigen I/II complex that is expressed by nearly all streptococci that inhabit the oral cavity. SspB is 1,500 residues in length and includes seven structural domains that are effectively maintained in all antigen I/II polypeptides. Previous studies in our group have shown that the region encompassing residues 1167 to 1250 of SspB (designated BAR for SspB adherence region) was required for the *in vitro* adherence of *P. gingivalis* to *S. gordonii* cells [15, 17–19]. From these studies, a peptide (designated BAR), was developed that potently inhibited *Pg* adherence to streptococci *in vitro* and reduced *Pg* virulence in a mouse model of periodontitis [15, 18, 19]. However, while BAR inhibited the initial formation of *Pg*/streptococcal biofilms, much higher concentrations of peptide were required to disrupt an established biofilm. In addition, disruption of more complex three-species biofilms containing a bridging organism such as *Fusobacterium nucleatum* also required higher concentration and prolonged exposure to BAR [20].

Currently, a variety of localized delivery approaches, including gels, implants, fibers, and films are used to deliver antibiotics. These formulations are often administered following the scaling process to retain antibiotics for prolonged duration in periodontal pockets. However, non-degradable implants such as nylon fibers [21], and acrylic and ethyl cellulose strips [22, 23] require surgical removal, while burst release of active agents is often observed after the administration of films and gels [24, 25]. Recently, polymeric nanoparticles have been investigated as a potential alternative to deliver active agents, due to their proven safety and biocompatibility. Moreover, in contrast to the ubiquitous activity of metallic NPs with inherent antimicrobial efficiency [26, 27], FDA-approved polymers such as poly(lactic-co-glycolic) acid (PLGA), have demonstrated biocompatibility and flexible tuning of physical properties, enabling tailored drug release and favorable dosing profiles [28]. In addition, polymer NPs have the ability to impart mucoadhesive properties due to the electrostatic interactions between NPs and gingival epithelium [28–30]. While a variety of polymer types can promote mucoadhesion, NPs synthesized from commonly used polymers, such as PLGA, may achieve mucoadhesion via hydrogen bonding, polymer entanglement with mucins, hydrophobic interactions, or a combination of these mechanisms [31, 32]. Furthermore, NP transport and internalization through the epithelium is dependent on particle size, surface charge, polymer hydrophobicity, mucoadhesivity, and the presence or absence of surface ligands like chitosan or PEG [13, 30, 31]. From a fabrication perspective, PLGA NPs are easily synthesized and provide long lasting formulations that can protect active agents, especially more labile biological agents, thereby maintaining their functional activity.

Given the attributes of PLGA NPs, we sought to address some of the delivery challenges confronting free BAR, including the relatively transient inhibition of *Pg* in the oral cavity and higher localized doses of BAR required to disrupt established biofilm [15, 18, 19, 33]. Multivalency is one option to improve the binding of BAR by enhancing the avidity and

Author Manuscript Author Manuscript Author Manuscript Author Manuscript

decreasing the detachment rate from *Pg* [34–36]. Previous studies have demonstrated that multivalently targeted NPs can improve binding, increase localized concentration and decrease the effective therapeutic doses and frequencies [24, 35, 37–39]. Previous work from our groups demonstrated that BAR-modified NPs (BNPs) delivered a high localized concentration of BAR peptide and improved the *in vitro* effectiveness of BAR through multivalent interactions with *P. gingivalis*, relative to free BAR [35]. Thus, we hypothesized that conjugating BAR to the NP surface may similarly decrease the therapeutic dose of BAR required to inhibit biofilm formation *in vivo* through multivalent binding to *P. gingivalis*, more effectively inhibiting oral biofilm formation [35, 38]. For oral administration, we administrated free BAR and BAR-modified NP with 2% carboxymethylcellulose to test BNPs against the "best" case adhesive formulations to improve retention in the oral cavity and to target *P. gingivalis*. In future work, we propose to incorporate BNPs in a mouthwash or gel formulation to be applied twice daily. Here our goal was to advance our previous *in vitro* work to assess the *in vivo* efficacy and safety of BAR-modified NPs in a murine model of periodontitis and in gingival and erythrocytic cell lines.

MATERIALS AND METHODS

Peptide Synthesis

BAR peptide is comprised of residues 1167 to 1193 of the SspB (Antigen I/II) protein of *S. gordonii* with the sequence NH_2-LEAAPKKVQDLLKKANITVKGAFQLFS-COOH [18]. To facilitate conjugation of BAR to the NP surface, the peptide was synthesized with an N-terminal biotin. Biotinylated BAR was subsequently attached to NPs that had been modified with palmitylated avidin. To enable peptide quantification and detection, some preparations of BAR were modified such that the epsilon amine of the underlined lysine residue of BAR was covalently reacted with 6-carboxyfluorescein to produce fluorescent BAR (F-BAR). All preparations of peptides were synthesized by BioSynthesis, Inc. (Lewisville, TX) and were guaranteed to have greater than 94% purity via RP-HPLC analysis.

BAR Surface-Modified Nanoparticle Synthesis

BAR surface-modified NPs were synthesized using a previously described single emulsion technique [39, 40]. PLGA with a 50:50 monomer ratio and 0.55–0.75 dL/g inherent viscosity, was purchased from LACTEL®. Briefly, 100 mg PLGA was dissolved in 2 mL dichloromethane (DCM) overnight. The following day, 2 mL of a 5% (w/v) polyvinyl alcohol (PVA) solution was mixed with 2 mL of 5 mg/mL avidin-palmitate. The 2 mL PLGA/DCM solution was added dropwise to 4 mL PVA/avidin-palmitate solution while vortexing. The NP solution was added to 50 mL of 0.3% PVA for 3 hr to evaporate residual DCM. After evaporation, the NP solution was centrifuged at 13,000 rpm (20,442 × g) at 4°C. Supernatant was discarded, and the pelleted NPs were resuspended in 10 mL phosphate buffered saline (PBS) for 30 min on a benchtop rotator, with biotinylated BAR peptide at a molar ratio of 6:1 BAR:avidin (18 nmol/mg) in PBS. After conjugation, the NPs were washed two times with deionized water (diH2O) by centrifugation at 13,000 rpm (20,442 × g) at 4°C to obtain NPs with sizes less than ~200 nm. After washing, BAR surface-modified NPs were suspended in 5 mL of diH2O, frozen at −80°C, and lyophilized. F-BAR-modified NPs were synthesized similarly, but were protected from light during synthesis.

Author Manuscript Author Manuscript Author Manuscript Author Manuscript

NP Characterization: NP Morphology, Size, BAR Conjugation

Unhydrated NP morphology, diameter, and size distribution were determined using scanning electron microscopy (SEM) (XL-30 ESEM-FEG SEM, FEI Company, USA). Lyophilized NPs were mounted on carbon tape and sputter coated with a thin layer of gold/palladium. Average diameters of 500 particles were determined from SEM images (n=3) using image analysis software (ImageJ, National Institutes of Health, version 1.5a, ImageJ.nih.gov). Dynamic light scattering and zeta potential analyses were performed to determine the hydrodynamic diameter and surface charge of hydrated NPs. The unhydrated and hydrated diameters of NPs are typically assessed to establish the size characteristics within different conditions of dry storage and more physiologically relevant aqueous environments. Briefly, a 1 mg/mL sample of BAR-modified PLGA NPs in diH2O was prepared. After vortexing and sonication, samples were diluted at a 1:50 ratio in diH2O. One mL was aliquoted to the cuvette for analysis [Malvern, Malvern, UK (Zetasizer Nano ZS90), courtesy of Dr. Martin O'Toole, Univ. of Louisville] to measure dynamic light scattering and zeta potential with Zetasizer Nano software. Samples were run in triplicate, using a refractive index of 1.57 for PLGA, absorption coefficient of 1, and water refractive index of 1.33. The equations used by the Zetasizer to calculate nanoparticle size are shown in Supplementary Data.

To measure the amount of BAR peptide that was conjugated to the NP surface, a fluorescence binding assay was conducted with F-BAR NPs. After conjugation, NPs were centrifuged and washed twice with diH2O to remove unbound BAR from the formulated NPs. NPs were then suspended in 1X PBS to create a 1 mg/mL NP solution and the resulting samples were transferred to a microtiter plate in triplicate. Total NP-associated fluorescence was determined using Victor3 Multilabel spectrophotometer (488/518 nm excitation/emission), and peptide quantity was determined from a standard curve of known F-BAR concentrations [35]. The stability of the avidin palmitate interaction with the NP surface has been previously tested by assessing the release of avidin and biotinylated ligand from the NP surface with respect to time [37, 41]. In addition, the functional stability of BNPs was tested through *in vitro* inhibition assays against biofilms prior to these *in vivo* experiments [35].

Growth of Bacterial Strains

P. gingivalis (ATCC 33277) was grown in Trypticase soy broth (Difco Laboratories Inc., Livonia, MI, USA) supplemented with 0.5% (w/v) yeast extract, 1 μg/mL menadione, and 5 μg/mL hemin. The medium was reduced for 24 hr under anaerobic conditions (10% CO_2, 10% H_2, and 80% N_2) and *P. gingivalis* was subsequently inoculated and grown anaerobically for 48 hr at 37°C. *S. gordonii* DL-1 was cultured aerobically without shaking in brain-heart infusion broth (Difco Laboratories Inc.) supplemented with 1% yeast extract for 16 hr at 37°C [15, 18, 19].

In Vivo Model of Periodontitis

The protocols used for the study were approved by the Institutional Animal Care and Use Committee (IACUC) at the University of Louisville, as described in the federal guidelines for the care and use of laboratory animals. Ten weeks-old specific-pathogen-free BALB/cByJ mice were obtained from the Jackson Laboratory (Bar Harbor, ME) and housed in the

Author Manuscript Author Manuscript Author Manuscript Author Manuscript

University of Louisville Research Resource Center animal facility. The mice were fed with Lab Diet 5001 meal (Purina Mills, LLC, Gray Summit, MO) during the entire experiment.

The oral infection of mice was performed as previously described [19]. A total of 8 mice per group were used per experiment. Animals were initially treated with sulfamethoxazole (MP Biomedical, Solon, OH) at a final concentration of (800 μg/mL) and trimethoprim (Sigma, St. Louis, MO) at a final concentration of (400 μg/mL) ad libitum for 10 days, every two days. Four days after the last antibiotic treatment, all groups of mice with the exception of the sham-infected control group were orally infected with 10^9 CFU of *S. gordonii* cells suspended in 1 mL of 2% carboxymethylcellulose (CMC; MP Biomedical, Solon, OH) in sterile PBS using a 2.25 mm feeding needle (Popper and Sons, Inc., New Hyde Park, NY). *Sg* was administered five times in total, every two days. Sham-infected animals received CMC without bacteria. Following confirmation of *Sg* colonization by PCR, two groups of animals were infected five times with 10^7 CFU of *P. gingivalis* in CMC containing BAR (0.7 and 3.4 μM) at two day intervals and another group was infected five times with 10^7 CFU of *Pg* in CMC containing BNPs (BAR concentration = 0.7 μM) at two day intervals. Two additional groups of animals were infected either with *Pg* alone or *Sg* alone. After the infection process, all animals were subsequently rested for 47 days with daily observation to record death or sickness and then euthanized via CO_2 asphyxiation.

Infection Confirmation

S. gordonii and *P. gingivalis* colonization were confirmed by collecting oral samples from the gingiva of the upper molars using a 15 cm sterile polyester-tipped applicator (Puritan Medical Products Co., Guilford, ME), 14 days after the last oral infection. Samples were then added to 10 mL of brain-heart infusion broth (Difco Laboratories Inc.) for streptococcal species enrichment and trypticase soy broth (Difco Laboratories Inc., Livonia, MI, USA) supplemented with 0.5% (w/v) yeast extract, 1 μg/mL menadione, and 5 μg/mL hemin to select for *Pg*. Samples were incubated at 37°C for 24 hr under anaerobic conditions. The resulting cells were identified by PCR using *S. gordonii*- and *P. gingivalis*-specific primers [19].

Determination of Maxillary Alveolar Bone Loss

Mouse skulls were autoclaved for 15 min to remove skin and muscles, and were subsequently soaked in 3% hydrogen peroxide overnight at room temperature to remove remaining muscle. Skulls were washed with diH2O and cleaned with a 1% bleach solution for 30 s, sonicated at 14 V for 1 min, and washed again with diH2O. To confirm skull cleaning, toothpaste was applied and brushed away, followed by immersion in a 1% bleach solution for 30 s and sonication (14 V). To stain the skulls, skulls were immersed in 1% methylene blue for 15 s and rinsed with DI water to remove excess dye. The stained skulls were air-dried prior to alveolar bone loss measurements. Bone loss was assessed by measuring the distance between the alveolar bone crest (ABC) and the cemento-enamel junction (CEJ) at 7 sites on the buccal side of the right and left maxillary molars for a total of 14 measurements. This was accomplished using a dissecting microscope fitted with a video imaging marker measurement system (model VIA-170K; Fryer) at a total magnification of 40x [19]. Measurements were taken in millimeters. The average of the total

Author Manuscript Author Manuscript Author Manuscript Author Manuscript

bone loss for each mouse group was assessed and subtracted from the baseline bone loss observed in sham-infected mice. Statistical differences in bone loss were analyzed by ANOVA after passing Bartlett's and Brown-Forsythe tests for homogeneity of variances using GraphPad InStat (La Jolla, CA). A pair-wise, parametric analysis of variance using a Bonferroni multiple comparison post-test was used to determine the statistical difference among the individual mouse groups. A P value of ≤ 0.05 was considered to be statistically significant.

Histological Analysis

Samples of maxillary molar regions were dissected from each mouse, and then fixed in 4% paraformaldehyde overnight. Periodontal tissues were dehydrated by passing through ascending concentrations of ethanol then cleared in xylene and embedded in paraffin. Serial sections (5–6 μm) were cut and mounted on glass slides (Sigma, St. Louis, MO). Microscopic examination for slides was carried out after hematoxylin and eosin staining [42].

Immunofluorescence Assay

An immunofluorescence assay was used to assess IL-17 expression in gingival sections. Tissue sections, 5–6 μm in thickness, were mounted on glass slides. Tissue sections were deparaffinized by immersion in xylol two times for 15 min each, and rehydrated in absolute, 95% and 70% ethanol. Excess ethanol was removed then slides were placed in water. Antigen IL-17 was recovered by microwave heating in water and non-specific binding was blocked with 5% bovine serum albumin for 1 hr. Then, slides were incubated for 24 hr at 4°C with IL-17A monoclonal antibody AlexaFluor 488 (eBioscience™), examined via confocal microscopy, and IL-17 immunofluorescence was quantified using Volocity software [43].

Tissue Culture

Telomerase immortalized gingival keratinocytes (TIGKs) were grown on 24-well collagen-coated plates (Becton Dickinson, Bedford, MA) and cultured using DermaLife K Calcium Free Medium (LifeFactors®) supplemented with penicillin/streptomycin (100 U/mL final concentration; St. Louis, MO), recombinant human (rh) insulin (5 μg/mL), L-glutamine (6 mM), epinephrine (1 μM), apo-transferrin (5 μg/mL), rh TGF-α (0.5 ng/ mL), extract P™, hydrocortisone hemisuccinate (100 ng/mL), and calcium chloride (0.06 mM). The epithelial cells were incubated at 37°C in the presence of 5% CO_2 for 6 days until they reached 95% confluence. The cells were washed and administered media without antibiotics during toxicity testing.

Determination of BAR and BNP *In Vitro* Cytotoxicity

Hemolytic Assay: A total of 250 μL of 1% sheep erythrocytes (Rockland Inc, Pennsylvania, USA) was suspended in sterile PBS containing 5% fetal bovine serum (FBS buffer). BNPs or free BAR peptide were suspended in FBS at concentrations of 1.3 and 3.4 μM (the maximum concentrations used in *in vitro* and *in vivo* studies) and were added to the erythrocyte suspension. The mixtures were incubated at 37°C for 3 hr. After centrifugation

Author Manuscript Author Manuscript Author Manuscript Author Manuscript

(3,500 × g), hemoglobin released due to cell lysis was analyzed by spectrophotometry at 541 nm. A positive control group was run in which PBS was replaced with diH2O.

MTT Assay: TIGK cells were seeded in 12-well plates at a density of 6×10^4 cells in 1 mL media per well, and incubated for 24 hr to allow for 60–70% confluency and sufficient adhesion. Cells were treated with 1.3 or 3.4 μM of free BAR or BNPs. After 24 hr, 100 μL of MTT solution (10% of total volume) was added to the media of all samples. The solution was incubated at 37°C for 4 hr. After this period, 550 μL of lysis buffer (50% of total volume) was added to the media of each well and plates were incubated for overnight. The absorbance of each well was read at 570 nm, and the sample absorbance was normalized to the absorbance of untreated cells (media only). Treatment with 10% DMSO media (100 μL DMSO in 900 μL media) was used as a positive control for cell death.

ATP Assay: Total ATP levels in cell culture were assessed by using the CellTiter-Glo reagent (Promega, Madison WI), as described by the manufacturer. TIGK cells were seeded at a density of 6×10^4 cells in 1 mL media per well and incubated at 37°C, 5% CO_2 for 24 hr in a 12-well flat bottom plate. Cells were then incubated with free BAR or BNPs (1.3 or 3.4 μM) for 24 hr at 37°C in 5% CO_2. Cells were then lysed with 500 μL of 0.1% Triton X-100 for 30 min at 37°C. The lysates were collected and centrifuged at 1,000 × g for 10 min at 4°C, and 50 μL of supernatant was mixed with 50 μL of CellTiter-Glo reagent. Samples were incubated at ambient temperature for 10 min in a black 96-well plate in the dark. Total luminescence was measured with a Victor 3 luminometer (Perkin-Elmer, Inc). Cells incubated with 1 ng of staurosporine or with medium only served as positive and negative controls for cell death, respectively.

LDH Assay: Cell membrane leakage was measured by the release of lactate dehydrogenase (LDH). Extracellular LDH was quantified using a CytoTox96® non-radioactive cytotoxicity assay (Promega, Madison WI) as described by the manufacturer. TIGK cells were plated at density of 6×10^4 cells in 1 mL media per well in a 12-well flat bottom plate, and incubated at 37°C, 5% CO_2 for 24 hr. Free BAR or BNPs (1.3 or 3.4 μM) were added to cells in triplicate for 24 hr at 37°C in 5% CO_2. Fifty microliters of supernatant from free BAR and BNP-treated (1.3 and 3.4 μM) cells were added to the LDH substrate and incubated at room temperature for 30 min. The reactions were subsequently terminated by adding 50 μL of stop solution. LDH activity was determined by measuring the optical density of the solution at 490 nm. Cells treated with staurosporine or with medium only served as positive and negative controls for cell death, respectively.

Apoptosis: The degree to which free BAR or BNPs (1.3 or 3.4 μM) induced apoptosis in TIGK cells was determined using the PE Annexin V/Dead Cell Apoptosis Kit with SYTOX® Green for Flow cytometry (Invitrogen). TIGK cells were cultured in 12-well microtiter plates with an initial density 2×10^5 cells in 1.5 ml media. After 24 hr at 37°C, the medium was decanted, replaced with fresh medium containing the desired concentration of BAR or BNPs and incubated for an additional 18 hr. The cells were washed with PBS, trypsinized and centrifuged at 250 × g. The cell pellet was suspended in 100 μL of binding buffer supplemented with 1 μL Sytox and 5 μL Annexin florescent dye and incubated for 15

Author Manuscript Author Manuscript Author Manuscript Author Manuscript

min at 37°C. Samples were then diluted by addition of 400 μL binding buffer and analyzed by flow cytometry using a FACScalibur flow cytometer (Becton Dickinson), measuring the fluorescence emission at 530 nm and 575 nm. Cells treated with 2 mM hydrogen peroxide or medium only for 4 hr at 37°C and 5% CO_2, served as positive and negative controls for apoptosis.

Statistical analysis

Data from each of the toxicity tests and IL-17 ELISA were analyzed using ANOVA after passing Bartlett's and Brown-Forsythe tests for homogeneity of variances using GraphPad InStat (La Jolla, CA). A pair-wise, parametric analysis of variance using a Bonferroni multiple comparison post-test was used to determine the statistical difference among the individual groups. A *P*-value of ≤ 0.05 was considered to be statistically significant.

RESULTS

Nanoparticle Characterization

The morphology of BNPs, relative to unmodified NPs, is shown in Figure 1. BNPs demonstrated a spherical morphology without any observed changes resulting from conjugation with BAR peptide. The average unhydrated diameters of BNPs and unmodified NPs measured from SEM images were 87.9 ± 29.4 nm and 155.8 ± 37.6 nm, respectively. In comparison, the average hydrated diameters of BNPs and unmodified NPs, as measured with dynamic light scattering (Malvern Zetasizer) were 333.8 ± 17.8 nm and 312.6 ± 11.2, respectively. This is in agreement with previous data demonstrating that BNP hydrated diameters were higher than unhydrated diameters [35]. The addition of positively charge avidin and subsequent conjugation with BAR increased the overall charge of BNPs to −10.3 ± 0.9 mV, relative to unmodified PLGA NPs (−22.6 ± 1.2 mV), demonstrating BAR conjugation to the PLGA NP surface (Table 1).

Quantification of BAR Conjugation

The amount of BAR peptide conjugated to PLGA NPs was determined using fluorescence spectroscopy, and the fluorescence was compared to a known standard of F-BAR. Previous work in our groups has shown that 3 nmol avidin conjugated per mg of PLGA NPs and avidin has four binding sites, with the potential to bind 12 nmol of BAR, if all avidin sites were available [35, 37, 44]. Loading experiments demonstrated that 7.1 nmol of BAR were bound per mg of PLGA NPs (corresponding to 9024 BAR ligands/mg of NP), with a conjugation efficiency 40%.

Alveolar Bone Loss

The effectiveness of free BAR and BNPs to inhibit *Pg* virulence was evaluated by measuring *Pg*-induced alveolar bone loss. Microscopic images of the maxilla of sham-infected, *Pg*/*Sg* infected, free BAR and BNP-treated mice are shown in Figure 2. Quantification of alveolar bone loss showed that mice that were infected with both *Sg* and *Pg* exhibited significantly (*P* ≤ 0.0001) increased bone loss (−1.37 ± 0.31 mm), relative to uninfected mice or animals infected with *Sg*-only (−0.33 ± 0.07 mm) or *Pg*-only (−0.44 ± 0.025 mm). Mice that were infected with both *Sg* and *Pg* and treated with 0.7 or 3.4 μM free BAR exhibited a significant

Author Manuscript Author Manuscript Author Manuscript Author Manuscript

reduction in bone loss (−0.69 ± 0.1 mm and −0.56 ± 0.09 mm, respectively), relative to infected untreated animals ($P \leq 0.0001$). Mice that were treated with 0.7 μM BNP exhibited levels of bone loss (−0.24 ± 0.05 mm) that approached uninfected animals. Moreover, 0.7 μM BNP-treated mice showed bone loss levels that were significantly lower than bone loss observed in 0.7 or 3.4 μM free BAR-treated mice ($P \leq 0.0001$and $P \leq 0.01$, respectively) (Figures 3).

Histological analysis

Representative histopathological images of gingival tissues of all mice are shown in Figure 4. Untreated uninfected gingival tissue shows normal structure without inflammatory cell infiltration. However, heavy infiltration of inflammatory cells and engorgement of blood vessel are observed in gingival tissue of *Pg* and *Sg* infected mice as a sign of chronic inflammation, as depicted with black arrows (Figure 4B). While, gingival tissues of free BAR and BNP-treated mice exhibit normal structure with minimal infiltration of inflammatory cells (Figure 4C–E), suggesting that free BAR and BNPs inhibit biofilm formation and consequently periodontitis. Mice treated with 0.7 μM BAR demonstrated higher levels of inflammatory cell infiltration relative to control mice; however, still lower than that observed in *Pg/Sg* infected mice.

IL-17 in Periodontal Tissues

To determine whether free BAR and BNPs reduced gingival inflammation, IL-17 levels in gingival tissues were evaluated across all treatment groups (see Figures 5A and 5B). The gingival tissue of *Pg*/*Sg* infected mice and mice treated with 0.7 μM free BAR demonstrated a statistically significant increase in IL-17 gingival tissue fluorescence (~2-fold, $P \leq 0.0001$ and ~1.5-fold, $P \leq 0.01$) relative to uninfected mice. In contrast, animals treated with 3.4 μM free BAR or with BNPs exhibited only a slight increase in IL-17 fluorescence (~1.13-fold), whereas mice treated with 0.7 μM free BAR showed a ~1.5-fold increase in IL-17 fluorescence significantly higher than BNP treated mice ($P \leq 0.05$). These results are consistent with the histological analysis of gingival tissues.

Determination of BAR and BAR-NP *In Vitro* Cytotoxicity

Hemolytic Assay: The cytotoxicity of free BAR and BNPs was initially evaluated by measuring the hemolytic activity against 1% sheep red blood cells (RBCs). As shown in Figure 6A, RBCs that were incubated with free BAR or BNPs (1.3 or 3.4 μM), or with PBS (control) showed no hemolysis, suggesting that free BAR or BNPs have negligible hemolytic activity in erythrocytes.

MTT Assay: To assess the effect of free BAR or BNPs on the viability of TIGK cells, cultures were incubated with 1.3 or 3.4 μM free BAR for 2 d and viability was measured using MTT. As shown in Figure 6B, treated cells exhibited little loss in viability, suggesting that free BAR and BNPs are biocompatible with TIGK cells when applied for up to 2 d.

ATP Assay: Cytotoxicity was also determined by assessing the metabolic activity of TIGK cells by measuring ATP levels. As shown in Figure 6C, staurosporine-treated cells demonstrated significantly lower levels of ATP ($P \leq 0.0001$) than were observed for

Author Manuscript Author Manuscript Author Manuscript Author Manuscript

uninfected, untreated; free BAR; and BNP-treated cells. Although the levels of ATP in free BAR and BNP-treated cells were statistically different from control cells, their levels were still elevated relative to staurosporine-treated cells.

LDH Assay: Since some peptides are known to damage the cell membrane, we next measured LDH activity as a marker for cell membrane integrity after treatment with free BAR or BNPs. Figure 6D shows that LDH levels released from cells treated with free BAR or BNPs (1.3 or 3.4 μM) was negligible when compared to control (medium treated) cells. In contrast, LDH activity released from cells treated with staurosporine was significantly ($P \leq 0.0001$) higher than control or treated cells, suggesting that free BAR and BNPs do not compromise cell membrane integrity. Finally, we examined the ability of free BAR or BNPs to induce apoptosis in TIGK cells. Flow cytometry results showed the presence of minimal apoptotic populations (lower right quadrant) when cells were incubated with 1.3 and 3.4 μM free BAR (3.5 and 14.9%, respectively) or BNPs (12.2 and 14.2%). In contrast, 89% of cells were apoptotic after treatment with 2 mM hydrogen peroxide (Figure 7, Table 2). These results indicate that free BAR and BNPs do not induce prominent apoptosis of TIGK cells.

DISCUSSION

Porphyromonas gingivalis adherence to oral streptococci is a key event in the initiation and pathogenesis of periodontal diseases, representing a specific target for therapeutic intervention [45]. Previous work in our groups has demonstrated that BAR peptide inhibits biofilm formation by preventing *P. gingivalis* adherence to streptococci *in vitro* and in a murine model of infection [16, 17]. However, the administration of free BAR was significantly less effective in disrupting existing *Pg*/streptococcal biofilms [15, 18, 19]. A recent study by our groups demonstrated the ability of BNPs to deliver a high concentration of peptide to potently and multivalently inhibit *in vitro* biofilm formation [35]. Given this, the aim of this work was to translate our previous *in vitro* BNP results to a murine model of periodontitis, highlighting the potential of novel specifically-targeted NPs in a prophylactic oral biofilm application.

Morphological characterization of BAR-modified PLGA NPs showed spherical NPs with an average diameter of 87.9 ± 29.4 nm and zeta potential of −10.3 ± 0.9 mV, while, the diameter and negative surface charge of unmodified NPs increased to 155.87± 37.6 nm and −22.6 ± 1.2 mV, respectively. The decrease in BNP size may be attributed to the increased surface charge imparted by avidin conjugation, which typically reduces aggregation, consequently decreasing NP size [46, 47]. The similar, but large increase in size of hydrated NPs, relative to unhydrated NPs, may be attributed to PLGA swelling in an aqueous solution [28, 47]. These results are in agreement with typically observed NP values [35, 47]. BNPs were fabricated using 18 nmol BAR per mg PLGA NP to provide maximum conjugation of BAR peptide (7.1 nmol/mg NPs) to the NP surface and the functional stability of BNPs relative to free BAR, was tested through *in vitro* biofilm inhibition assays prior to these *in vivo* experiments.

To expand upon our *in vitro* studies, we assessed the efficacy of BNPs, relative to free BAR, to prevent alveolar bone loss in a mouse model of periodontitis. Mice infected with *Pg* and

Author Manuscript Author Manuscript Author Manuscript Author Manuscript

Sg showed significantly increased bone loss relative to that observed in untreated, uninfected mice, or animals infected with *Sg* or *Pg* alone. Treatment with either free BAR or BNPs significantly reduced bone loss in *Pg*/*Sg* infected mice. Treatment with 0.7 μM or 3.4 μM free BAR reduced bone loss in a dose-dependent manner, but interestingly, treatment with 0.7 μM BNPs reduced bone loss to a significantly greater extent than either dose of free BAR. This is consistent with our previous *in vitro* observations that BNPs promote multivalent interactions with *Pg* [35]. The reduction of bone loss arose from reduced *Pg*-induced gingival inflammation that most likely occurred through BNP-mediated inhibition of *Pg* colonization of the oral cavity.

In corroboration with efficacy data, histopathological examination of gingival tissues showed minor levels of inflammatory cell infiltration in the gingiva of uninfected animals but significantly increased inflammatory cell infiltration in the gingiva of *Pg/Sg* infected mice. Consistent with the bone loss data, treatment with free BAR or BNPs significantly reduced inflammation. In addition, gingival tissue levels of the pro-inflammatory cytokine, IL-17, were significantly increased upon infection and significantly reduced upon treatment. Finally, free BAR and BNPs exhibited minimal toxicity against TIGK cells using various approaches to assess cell lysis, induction of apoptosis, or effects of cell viability or metabolism. Together, these results indicate the utility of BNPs to provide and enhance protection in a murine model of periodontitis, relative to treatment with free BAR.

To date, a variety of groups have developed polymeric delivery vehicles to improve traditional treatment and prevention approaches to periodontal diseases [48]. However, polymeric delivery vehicles have been primarily developed to deliver antibiotics [48–52] for prolonged durations, and to decrease antibiotic dose, administration frequency, and associated adverse effects. However, antibacterial resistance and non-specificity still remain challenges to effectively eradicate initial and recurrent biofilms, pathogen resistance, and associated diseases [8–10] . While recent studies have demonstrated some success using various polymeric NPs in dental pathogen murine models [48, 49], these studies have focused on targeting antibiotic NP formulations to epithelial cells with gingival targeting RGD peptides. Results from these studies indicated that NP surface-modification improved NP attachment to epithelial cells, maintaining antibacterial (i.e., minocycline) concentrations in gingival fluid for prolonged durations and improved therapeutic activity relative to unmodified NPs [24]. Other studies have similarly sought to use RGD [24], or more general bioadhesive molecules such as chitosan [53, 54] or dimethyloctyl ammonium [38], to obtain improved localization and adhesion to the dental surface. Strong mucoadhesive properties and adhesion to the tooth surface were demonstrated for antibacterial NPs modified with these agents [53].

Although non-specific mucoadhesive molecules and broad targeting molecules such as RGD have demonstrated promise in establishing adhesion, the challenges surrounding antibiotic active agents have spurred the discovery and investigation of specifically-targeted molecules against oral biofilms. Antimicrobial peptide (HHC-36) loaded titanium oxide nanotubes, titanium binding peptide (TiBP-1), histatin 5, and lactoferricin peptides have been developed to enhance pre-implant protection against bacterial infection and prevent biofilm formation [55–57]. In addition, a terminal product of the cyclooxygenase (COX)-2 pathway (15d-

Author Manuscript Author Manuscript Author Manuscript Author Manuscript

PGJ2) has been administered to inhibit bone resorption *in vivo* [14]. PLGA NPs, encapsulating 15d-PGJ2, localized in gingival tissue, showed potent anti-inflammatory response by decreasing proinflammatory cytokines, demonstrated immunomodulatory effects, and decreased bone resorption in a mouse model of periodontitis after daily s.c. injection [14].

In contrast with the non-specific bioadhesive and targeting developments described above, the goal of this work was to incorporate a pathogen-specific biological active agent within a surface modification, to exploit the specific and adhesive interactions between two bacteria known to initiate the process of periodontal infections. Previous *in vitro* studies conducted by our group have demonstrated that BAR-modified NPs exhibit potent biofilm inhibition with a 7-fold lower IC50, relative to free BAR [35], highlighting the benefits of a multivalent delivery system to enhance binding to target sites. Seminal work in the area of multivalency demonstrated that multivalent ligands can enhance the strength or binding avidity to target sites, relative to that observed with monovalent ligands, by increasing the affinity to target entities while decreasing detachment rates [36, 39, 58]. Our prior *in vitro* results with BNPs are consistent with the enhanced binding anticipated via these mechanisms, demonstrating improved effectiveness, with lower BAR concentration. Importantly, results from our current *in vivo* studies corroborate the *in vitro* multivalent effects, by demonstrating that 0.7 μM BAR, conjugated to a NP surface, safely and significantly reduces bone loss and inflammation, relative to a higher concentration of monovalent free BAR (3.4 μM), in a murine model of infection. Moreover, BAR NPs, within the range of concentrations examined in this study, provide a safe method, as assessed with four different studies, to induce biofilm inhibition. The use of biodegradable FDA-approved polymers, such as PLGA, as a core platform, offers the potential for the incorporation of other complementary active agents, and more seamless integration in pre-clinical and clinical studies. Ongoing studies in our group will utilize these particles in dual capacity to both multivalently target specific species of bacteria and to release active agents simultaneously.

In future studies, we intend to examine different temporal administration regimens to optimize prevention and treatment approaches with this platform. In addition, we plan to extend our studies to assess the kinetics of BNPs in the oral cavity after gingival application, and correlate this with BNP effectiveness in preventing (or treating) biofilm formation. Moreover, we will evaluate the stability and longevity of BNP binding with *Pg* in the oral cavity. Long-term, clinical studies will focus on formulating BNPs to more conveniently apply BNPs to the oral cavity, for example, in a mouthwash or gel, with the goal of retaining BNPs in oral niches for durations spanning 12–24 hr. While existing products designed for localized periodontal prevention and treatment contain antibiotics, analgesic, or anesthetic cargos, we envision that this technology may offer a new way to deliver specifically-acting biologics to the oral cavity.

CONCLUSIONS

Building upon our previous *in vitro* work, the goal of these studies was to assess the *in vivo* efficacy and safety of BNPs in a murine model of periodontitis. We hypothesized that BNPs may more potently and safely inhibit *Pg* virulence *in vivo* by delivering a high localized

Author Manuscript Author Manuscript Author Manuscript Author Manuscript

concentration of BAR, and improving BAR effectiveness through multivalent interactions with *Pg*. The *in vivo* efficacy of BNPs was evaluated in a periodontitis murine model by measuring bone loss, histologic changes, and gingival IL-17 expression as outcomes of *Pg*-induced inflammation. The safety of BNPs was evaluated by measuring cell viability, apoptosis, ATP and LDH levels in TIGK cells and hemolytic activity in sheep erythrocytes. BNPs significantly reduced bone loss and IL-17 expression in *Pg/Sg* infected mice to levels of sham-infected mice, and to a greater extent than an equimolar amount of free BAR. Moreover, BNPs and free BAR showed non-hemolytic activity and demonstrated greater than 90% viability, with apoptosis, ATP and LDH levels similar to untreated cells. Our results suggest that BNPs provide a potent platform to inhibit *Pg* virulence, relative to free BAR, while eliciting a safe, non-toxic effect within the evaluated concentration range of 1.3 – 3.4 μM on gingival and erythrocytic cells, suggesting this novel therapeutic approach for delivery to the oral cavity.

Supplementary Material

Refer to Web version on PubMed Central for supplementary material.

ACKNOWLEDGEMENTS

This work was supported by grants R01DE023206 and R21DE025345 from the National Institute for Dental and Craniofacial Research. The authors declare no conflicts of interest. We will freely provide reagents and/or data generated in this study to academic investigators according to the policies of the University of Louisville. An abstract comprised of parts of this study was presented on March 24, 2017 at the International Association of Dental Research Meeting in San Francisco, CA. In addition, other parts of this work were presented on July 24, 2018 at the annual Controlled Release Society Meeting, NY and on August 2, 2018 at the KY Nano/AM Symposium in Louisville, KY.

REFERENCES

[1]. Genco RJ, Van Dyke TE. Prevention: Reducing the risk of CVD in patients with periodontitis. Nature reviews Cardiology 2010;7:479–80.

[2]. Lundberg K, Wegner N, Yucel-Lindberg T, Venables PJ. Periodontitis in RA-the citrullinated enolase connection. Nature reviews Rheumatology 2010;6:727–30. [PubMed: 20820197]

[3]. Hajishengallis G, Lamont RJ. Beyond the red complex and into more complexity: the polymicrobial synergy and dysbiosis (PSD) model of periodontal disease etiology. Molecular oral microbiology 2012;27:409–19. [PubMed: 23134607]

[4]. Hajishengallis G, Liang S, Payne MA, Hashim A, Jotwani R, Eskan MA, et al. Low-abundance biofilm species orchestrates inflammatory periodontal disease through the commensal microbiota and complement. Cell host & microbe 2011;10:497–506. [PubMed: 22036469]

[5]. Honda K Porphyromonas gingivalis sinks teeth into the oral microbiota and periodontal disease. Cell host & microbe 2011;10:423–5. [PubMed: 22100158]

[6]. Kimura S, Nagai A, Onitsuka T, Koga T, Fujiwara T, Kaya H, et al. Induction of experimental periodontitis in mice with Porphyromonas gingivalis-adhered ligatures. Journal of periodontology 2000;71:1167–73. [PubMed: 10960025]

[7]. Maresz KJ, Hellvard A, Sroka A, Adamowicz K, Bielecka E, Koziel J, et al. Porphyromonas gingivalis facilitates the development and progression of destructive arthritis through its unique bacterial peptidylarginine deiminase (PAD). PLoS pathogens 2013;9:e1003627. [PubMed: 24068934]

[8]. Allaker RP, Ian Douglas CW. Non-conventional therapeutics for oral infections. Virulence 2015;6:196–207. [PubMed: 25668296]

Author Manuscript Author Manuscript Author Manuscript Author Manuscript

[9]. Drisko CH. Non-surgical pocket therapy: pharmacotherapeutics. Annals of periodontology 1996;1:491–566. [PubMed: 9118269]

[10]. Walker CB. The acquisition of antibiotic resistance in the periodontal microflora. Periodontology 2000 1996;10:79–88. [PubMed: 9567938]

[11]. Tiyaboonchai W, Rodleang I, Ounaroon A. Mucoadhesive polyethylenimine-dextran sulfate nanoparticles containing Punica granatum peel extract as a novel sustained-release antimicrobial. Pharmaceutical development and technology 2015;20:426–32. [PubMed: 24438035]

[12]. Moulari B, Lboutounne H, Chaumont JP, Guillaume Y, Millet J, Pellequer Y. Potentiation of the bactericidal activity of Harungana madagascariensis Lam. ex Poir. (Hypericaceae) leaf extract against oral bacteria using poly (D, L-lactide-co-glycolide) nanoparticles: in vitro study. Acta odontologica Scandinavica 2006;64:153–8. [PubMed: 16809192]

[13]. Liu L, Shu S, Cheung GS, Wei X. Effect of miR-146a/bFGF/PEG-PEI Nanoparticles on Inflammation Response and Tissue Regeneration of Human Dental Pulp Cells. BioMed research international 2016;2016:3892685. [PubMed: 27057540]

[14]. Napimoga MH, da Silva CA, Carregaro V, Farnesi-de-Assuncao TS, Duarte PM, de Melo NF, et al. Exogenous administration of 15d-PGJ2-loaded nanocapsules inhibits bone resorption in a mouse periodontitis model. Journal of immunology 2012;189:1043–52.

[15]. Daep CA, James DM, Lamont RJ, Demuth DR. Structural characterization of peptide-mediated inhibition of Porphyromonas gingivalis biofilm formation. Infection and immunity 2006;74:5756–62. [PubMed: 16988253]

[16]. Lamont RJ, El-Sabaeny A, Park Y, Cook GS, Costerton JW, Demuth DR. Role of the Streptococcus gordonii SspB protein in the development of Porphyromonas gingivalis biofilms on streptococcal substrates. Microbiology 2002;148:1627–36. [PubMed: 12055284]

[17]. Park Y, Simionato MR, Sekiya K, Murakami Y, James D, Chen W, et al. Short fimbriae of Porphyromonas gingivalis and their role in coadhesion with Streptococcus gordonii. Infection and immunity 2005;73:3983–9. [PubMed: 15972485]

[18]. Daep CA, Lamont RJ, Demuth DR. Interaction of Porphyromonas gingivalis with oral streptococci requires a motif that resembles the eukaryotic nuclear receptor box protein-protein interaction domain. Infection and immunity 2008;76:3273–80. [PubMed: 18474648]

[19]. Daep CA, Novak EA, Lamont RJ, Demuth DR. Structural dissection and in vivo effectiveness of a peptide inhibitor of Porphyromonas gingivalis adherence to Streptococcus gordonii. Infection and immunity 2011;79:67–74. [PubMed: 21041492]

[20]. Bradshaw DJ, Marsh PD, Watson GK, Allison C. Role of Fusobacterium nucleatum and coaggregation in anaerobe survival in planktonic and biofilm oral microbial communities during aeration. Infection and immunity 1998;66:4729–32. [PubMed: 9746571]

[21]. Ahuja AAJ, Shareef A, Khar R. Formulation and development of targeted retentive device for the treatment of periodontal infections with amoxycillin trihydrate. Indian J Pharm Sci 2006;68:6.

[22]. Somayaji BV, Jariwala U, Jayachandran P, Vidyalakshmi K, Dudhani RV. Evaluation of antimicrobial efficacy and release pattern of tetracycline and metronidazole using a local delivery system. Journal of periodontology 1998;69:409–13. [PubMed: 9609369]

[23]. Wade WG, Moran J, Morgan JR, Newcombe R, Addy M. The effects of antimicrobial acrylic strips on the subgingival microflora in chronic periodontitis. Journal of clinical periodontology 1992;19:127–34. [PubMed: 1602037]

[24]. Yao W, Xu P, Zhao J, Ling L, Li X, Zhang B, et al. RGD functionalized polymeric nanoparticles targeting periodontitis epithelial cells for the enhanced treatment of periodontitis in dogs. Journal of colloid and interface science 2015;458:14–21. [PubMed: 26197107]

[25]. Tonetti MS, Pini-Prato G, Cortellini P. Principles and clinical applications of periodontal controlled drug delivery with tetracycline fibers. The International journal of periodontics & restorative dentistry 1994;14:421–35. [PubMed: 7751109]

[26]. Lu Z, Rong K, Li J, Yang H, Chen R. Size-dependent antibacterial activities of silver nanoparticles against oral anaerobic pathogenic bacteria. Journal of materials science Materials in medicine 2013;24:1465–71. [PubMed: 23440430]

Author Manuscript Author Manuscript Author Manuscript Author Manuscript

[27]. Martinez-Gutierrez F, Thi EP, Silverman JM, de Oliveira CC, Svensson SL, Vanden Hoek A, et al. Antibacterial activity, inflammatory response, coagulation and cytotoxicity effects of silver nanoparticles. Nanomedicine : nanotechnology, biology, and medicine 2012;8:328–36.

[28]. Makadia HK, Siegel SJ. Poly Lactic-co-Glycolic Acid (PLGA) as Biodegradable Controlled Drug Delivery Carrier. Polymers 2011;3:1377–97. [PubMed: 22577513]

[29]. de Freitas LM, Calixto GM, Chorilli M, Giusti JS, Bagnato VS, Soukos NS, et al. Polymeric Nanoparticle-Based Photodynamic Therapy for Chronic Periodontitis in Vivo. International journal of molecular sciences 2016;17.

[30]. Patel A, Patel M, Yang X, Mitra AK. Recent advances in protein and Peptide drug delivery: a special emphasis on polymeric nanoparticles. Protein and peptide letters 2014;21:1102–20. [PubMed: 25106908]

[31]. Ensign LM, Cone R, Hanes J. Oral drug delivery with polymeric nanoparticles: the gastrointestinal mucus barriers. Advanced drug delivery reviews 2012;64:557–70. [PubMed: 22212900]

[32]. Lai SK, Wang YY, Hanes J. Mucus-penetrating nanoparticles for drug and gene delivery to mucosal tissues. Advanced drug delivery reviews 2009;61:158–71. [PubMed: 19133304]

[33]. Mahmoud MY, Demuth DR, Steinbach-Rankins JM. BAR-encapsulated nanoparticles for the inhibition and disruption of Porphyromonas gingivalis-Streptococcus gordonii biofilms. Journal of nanobiotechnology 2018;16:69. [PubMed: 30219060]

[34]. Fasting C, Schalley CA, Weber M, Seitz O, Hecht S, Koksch B, et al. Multivalency as a chemical organization and action principle. Angewandte Chemie 2012;51:10472–98. [PubMed: 22952048]

[35]. Kalia P, Jain A, Radha Krishnan R, Demuth DR, Steinbach-Rankins JM. Peptide-modified nanoparticles inhibit formation of Porphyromonas gingivalis biofilms with Streptococcus gordonii. International journal of nanomedicine 2017;12:4553–62. [PubMed: 28790818]

[36]. Mammen M, Choi SK, Whitesides GM. Polyvalent Interactions in Biological Systems: Implications for Design and Use of Multivalent Ligands and Inhibitors. Angewandte Chemie 1998;37:2754–94. [PubMed: 29711117]

[37]. Fahmy TM, Samstein RM, Harness CC, Mark Saltzman W. Surface modification of biodegradable polyesters with fatty acid conjugates for improved drug targeting. Biomaterials 2005;26:5727–36. [PubMed: 15878378]

[38]. Zaltsman N, Ionescu AC, Weiss EI, Brambilla E, Beyth S, Beyth N. Surface-modified nanoparticles as anti-biofilm filler for dental polymers. PloS one 2017;12:e0189397. [PubMed: 29244848]

[39]. Sims LB, Curtis LT, Frieboes HB, Steinbach-Rankins JM. Enhanced uptake and transport of PLGA-modified nanoparticles in cervical cancer. Journal of nanobiotechnology 2016;14:33. [PubMed: 27102372]

[40]. Martin DT, Steinbach JM, Liu J, Shimizu S, Kaimakliotis HZ, Wheeler MA, et al. Surface-modified nanoparticles enhance transurothelial penetration and delivery of survivin siRNA in treating bladder cancer. Molecular cancer therapeutics 2014;13:71–81. [PubMed: 24222663]

[41]. Park J, Mattessich T, Jay SM, Agawu A, Saltzman WM, Fahmy TM. Enhancement of surface ligand display on PLGA nanoparticles with amphiphilic ligand conjugates. Journal of controlled release : official journal of the Controlled Release Society 2011;156:109–15.

[42]. Garlet GP, Avila-Campos MJ, Milanezi CM, Ferreira BR, Silva JS. Actinobacillus actinomycetemcomitans-induced periodontal disease in mice: patterns of cytokine, chemokine, and chemokine receptor expression and leukocyte migration. Microbes and infection 2005;7:738–47. [PubMed: 15850760]

[43]. Rojo-Botello NR, Garcia-Hernandez AL, Moreno-Fierros L. Expression of toll-like receptors 2, 4 and 9 is increased in gingival tissue from patients with type 2 diabetes and chronic periodontitis. Journal of periodontal research 2012;47:62–73. [PubMed: 21848608]

[44]. Howarth M, Chinnapen DJ, Gerrow K, Dorrestein PC, Grandy MR, Kelleher NL, et al. A monovalent streptavidin with a single femtomolar biotin binding site. Nature methods 2006;3:267–73. [PubMed: 16554831]

[45]. Ellen RP. Periodontal care for community-dwelling older adults. The Journal of prosthetic dentistry 1994;72:500–6. [PubMed: 7844752]

Author Manuscript Author Manuscript Author Manuscript Author Manuscript

[46]. Hotze EM, Phenrat T, Lowry GV. Nanoparticle aggregation: challenges to understanding transport and reactivity in the environment. Journal of environmental quality 2010;39:1909–24. [PubMed: 21284288]

[47]. Steinbach JM, Seo YE, Saltzman WM. Cell penetrating peptide-modified poly(lactic-co-glycolic acid) nanoparticles with enhanced cell internalization. Acta biomaterialia 2016;30:49–61. [PubMed: 26602822]

[48]. Yao W, Xu P, Pang Z, Zhao J, Chai Z, Li X, et al. Local delivery of minocycline-loaded PEG-PLA nanoparticles for the enhanced treatment of periodontitis in dogs. International journal of nanomedicine 2014;9:3963–70. [PubMed: 25170266]

[49]. Horev B, Klein MI, Hwang G, Li Y, Kim D, Koo H, et al. pH-activated nanoparticles for controlled topical delivery of farnesol to disrupt oral biofilm virulence. ACS nano 2015;9:2390–404. [PubMed: 25661192]

[50]. Pinon-Segundo E, Ganem-Quintanar A, Alonso-Perez V, Quintanar-Guerrero D. Preparation and characterization of triclosan nanoparticles for periodontal treatment. International journal of pharmaceutics 2005;294:217–32. [PubMed: 15814246]

[51]. Qin Y, Yuan M, Li L, Li W, Xue J. Formulation and evaluation of in situ forming PLA implant containing tinidazole for the treatment of periodontitis. Journal of biomedical materials research Part B, Applied biomaterials 2012;100:2197–202.

[52]. Lee BS, Lee CC, Wang YP, Chen HJ, Lai CH, Hsieh WL, et al. Controlled-release of tetracycline and lovastatin by poly(D,L-lactide-co-glycolide acid)-chitosan nanoparticles enhances periodontal regeneration in dogs. International journal of nanomedicine 2016;11:285–97. [PubMed: 26848264]

[53]. Chronopoulou L, Nocca G, Castagnola M, Paludetti G, Ortaggi G, Sciubba F, et al. Chitosan based nanoparticles functionalized with peptidomimetic derivatives for oral drug delivery. New biotechnology 2016;33:23–31. [PubMed: 26257139]

[54]. Takahashi C, Akachi Y, Ogawa N, Moriguchi K, Asaka T, Tanemura M, et al. Morphological study of efficacy of clarithromycin-loaded nanocarriers for treatment of biofilm infection disease. Medical molecular morphology 2017;50:9–16. [PubMed: 27119723]

[55]. Ma M, Kazemzadeh-Narbat M, Hui Y, Lu S, Ding C, Chen DD, et al. Local delivery of antimicrobial peptides using self-organized TiO2 nanotube arrays for peri-implant infections. Journal of biomedical materials research Part A 2012;100:278–85. [PubMed: 22045618]

[56]. Yazici H, O'Neill MB, Kacar T, Wilson BR, Oren EE, Sarikaya M, et al. Engineered Chimeric Peptides as Antimicrobial Surface Coating Agents toward Infection-Free Implants. ACS applied materials & interfaces 2016;8:5070–81. [PubMed: 26795060]

[57]. Yoshinari M, Kato T, Matsuzaka K, Hayakawa T, Shiba K. Prevention of biofilm formation on titanium surfaces modified with conjugated molecules comprised of antimicrobial and titanium-binding peptides. Biofouling 2010;26:103–10. [PubMed: 20390560]

[58]. Li MH, Zong H, Leroueil PR, Choi SK, Baker JR, Jr. Ligand Characteristics Important to Avidity Interactions of Multivalent Nanoparticles. Bioconjugate chemistry 2017;28:1649–57. [PubMed: 28398751]

Author Manuscript Author Manuscript Author Manuscript Author Manuscript

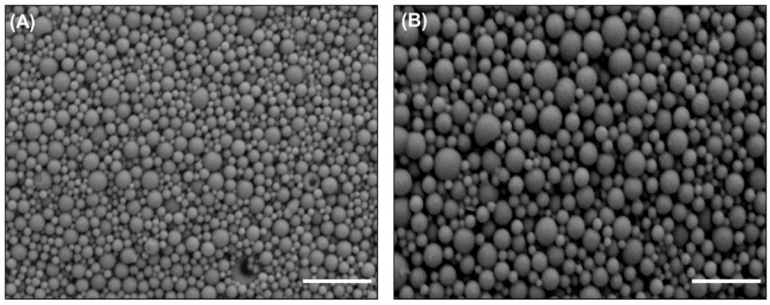

Figure 1.

SEM images of (A) BAR-modified PLGA NPs and (B) Unmodified PLGA NPs. Scale bar represents 1 μm. Images are representative of a minimum of 3 independent samples, with n > 500 NPs assessed in total.

Author Manuscript Author Manuscript Author Manuscript Author Manuscript

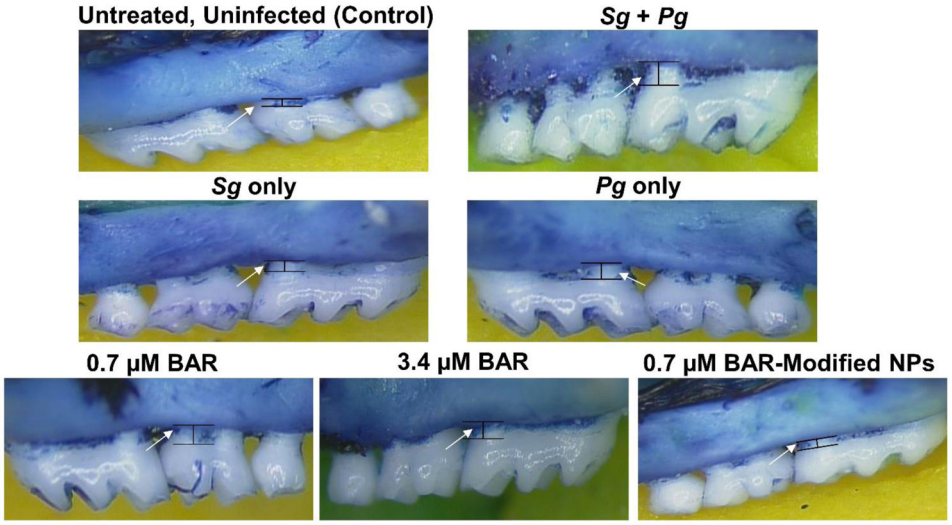

Figure 2.

Representative images from different *in vivo* treatment groups (n=8 per group), of the area between the cemento-enamel junction (CEJ) and alveolar bone crest (ABC), measured to determine bone loss. Images were taken using a dissecting microscope fitted with a video imaging marker measurement system (Sony model VIA −170K; Fryer) at a total magnification of 40x.

Author Manuscript Author Manuscript Author Manuscript Author Manuscript

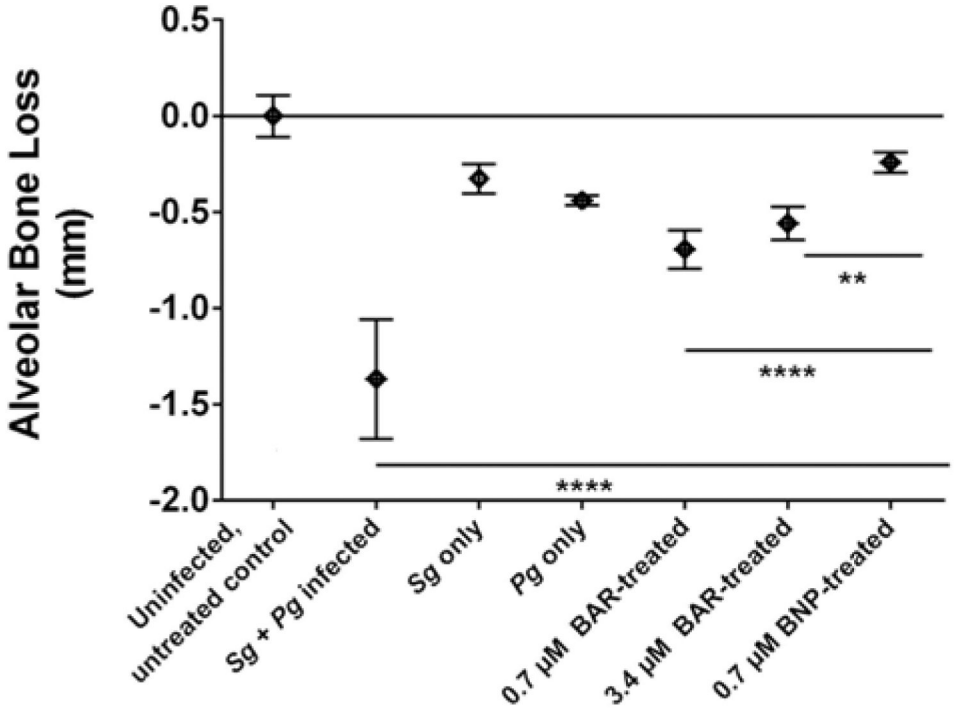

Figure 3.

Alveolar bone loss in each group relative to uninfected, untreated control mice. BNP-treated mice showed significant reduction of bone loss relative to high and low concentrations of free BAR-treated mice. Data represent the mean ± standard deviation (n=8). Statistical differences between groups are denoted by **, $P \leq 0.01$; ****, $P \leq 0.0001$).

Author Manuscript Author Manuscript Author Manuscript Author Manuscript

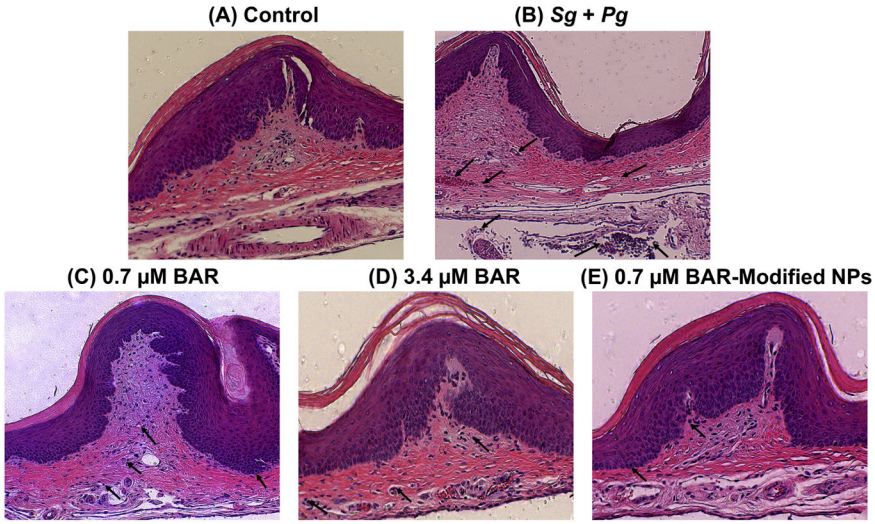

Figure 4.

Histological sections of murine periodontal tissues, with inflammatory cell infiltration denoted with black arrows. (A) Periodontal tissue of uninfected, untreated (control) mice shows normal histological structure without inflammatory cell infiltration. (B) Periodontal tissue of *Pg/Sg* infected mice demonstrates prominent chronic inflammation through proliferation of connective tissue and heavy infiltration of inflammatory cells. (C) Periodontal tissue of mice treated with 0.7 μM BAR exhibits medium infiltration of inflammatory cells. (D) & (E) Periodontal tissues treated with a higher concentration of free BAR (3.4 μM) or BNPs show normal histological structure with minimal infiltration of inflammatory cells. (H&E, 100x).

Author Manuscript Author Manuscript Author Manuscript Author Manuscript

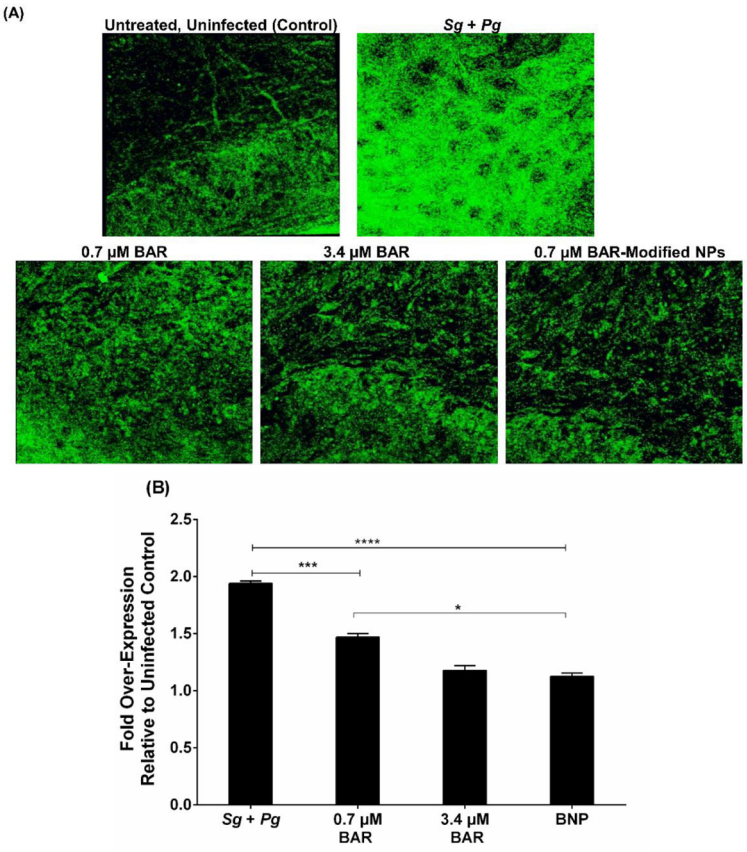

Figure 5.

(A) Immunofluorescence staining of IL-17 on gingival tissue demonstrated strong staining of the *Pg* and *Sg* infected group compared to the uninfected, untreated; 0.7 μM BAR; 3.4 μM BAR; and BNP-treated groups. (B) Quantification of IL-17 levels show that free BAR and BNP-treated groups had similar IL-17 expression relative to the untreated, uninfected mice; however, mice treated with a lower concentration (0.7 μM) of free BAR showed slightly higher, statistically significant IL-17 levels relative to untreated, uninfected and BNP-treated mice. Data represent the mean ± standard deviation (n=5); (*, $P \leq 0.05$, ***, $P \leq 0.001$ ****, $P \leq 0.0001$).

Author Manuscript Author Manuscript Author Manuscript Author Manuscript

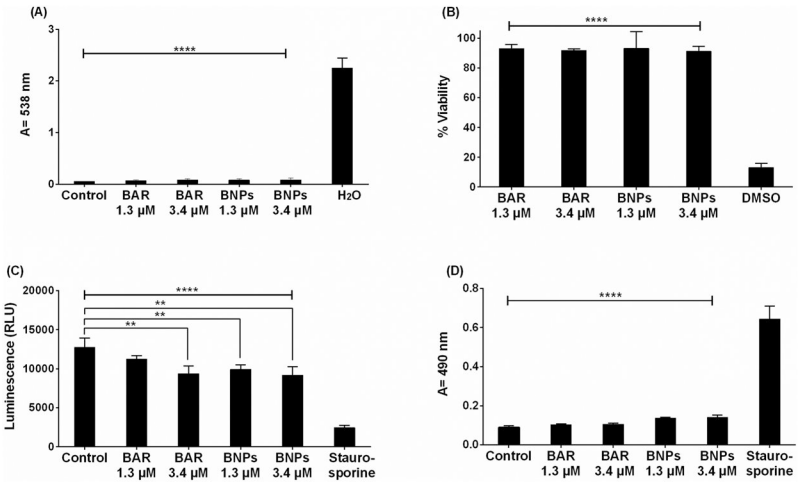

Figure 6.

(A) The hemolytic activity of free BAR or BNPs (1.3, 3.4 μM) was assessed after administration to sheep erythrocytes for 3 hr. Hemoglobin release from free BAR and BNP-treated cells was negligible relative to release from H_2O-treated cells (****, $P \leq 0.0001$). (B) TIGK cell viability was assessed after free BAR or BNPs (1.3, 3.4 μM) administration for 2 days. Free BAR and BNPs were non-toxic, relative to cells treated with DMSO (****, $P \leq 0.0001$). (C) ATP levels from free BAR (3.4 μM) and BNP-treated (1.3, 3.4 μM) cells showed decreases in ATP concentration, relative to control cells (treated with medium only), while ATP levels in the staurosporine-treated cells were significantly lower than the control (treated with medium only), free BAR, and BNP-treated cells (****, $P \leq 0.0001$). (D) Cell membrane damage induced by free BAR or BNPs (1.3, 3.4 μM) was assessed by measuring LDH levels. No significant release of LDH was observed from TIGK cells treated with free BAR and BNPs, relative to control cells (treated with media only). Staurosporine-treated cells demonstrated significantly elevated LDH levels (****, $P \leq 0.0001$). Data represent the mean ± standard deviation (n=5).

Author Manuscript Author Manuscript Author Manuscript Author Manuscript

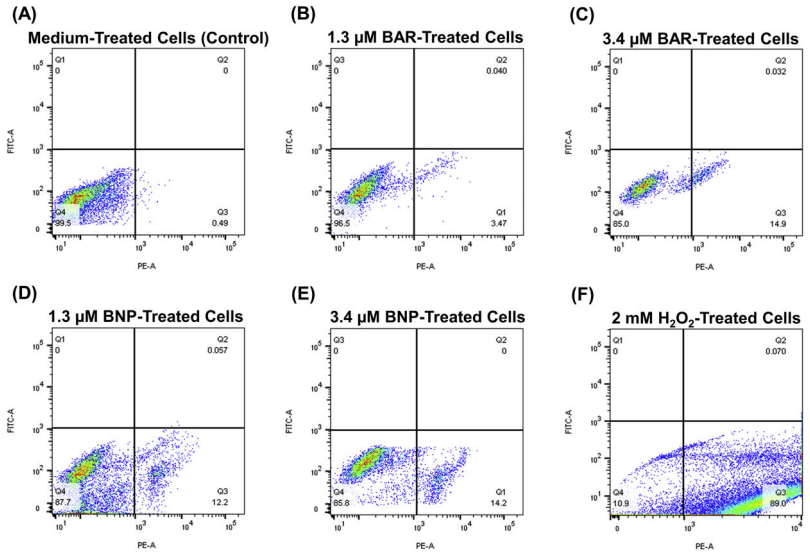

Figure 7.

TIGK cells were treated with (A) medium alone, (B) 1.3 μM free BAR, (C) 3.4 μM free BAR, (D) 1.3 μM BNPs, (E) 3.4 μM BNPs and (F) 2 mM hydrogen peroxide. The FITC versus phycoerythrin (PE) fluorescence dot plots show the live (bottom left quadrant) and apoptotic cell (bottom right quadrant) cell populations. Data represent the mean ± standard deviation (n=3), 10,000 counts.

Author Manuscript

Author Manuscript

Author Manuscript

Author Manuscript

Table 1.

Physical characterization of NP diameter and surface charge. Data represent the mean ± S.D. of at least 3 independent samples.

NP Type	Unhydrated Diameter (nm)	Hydrated Diameter (nm)	Zeta Potential (mV)
BAR-Modified PLGA NPs	87.9 ± 29.4	333.8 ± 17.8	−10.3 ± 0.9
Unmodified PLGA NPs	155.87± 37.6	312.6 ± 11.2	−22.6 ± 1.2

Author Manuscript

Author Manuscript

Author Manuscript

Author Manuscript

Table 2.

TIGK cells apoptosis induced by 1.3 μM free BAR, 3.4 μM free BAR, 1.3 μM BNPs, 3.4 μM BNPs and 2 mM hydrogen peroxide relative to cells treated with medium alone, (*, $P \leq 0.05$, **, $P \leq 0.01$ and ***, $P \leq 0.001$).

Treatment	% Live Cell	% Early Apoptosis	% Late Apoptosis
Medium	99.00 ± 1.22	0.80 ± 0.56	0.097 ± 0.06
BAR 1.3 μM	95.60 ± 1.01	3.39 ± 0.17	0.18 ± 0.09
BAR 3.4 μM	84.07 ± 0.81*	15.33 ± 0.51*	0.41 ± 0.24
BNPs 1.3 μM	86.57 ± 2.23*	12.53 ± 1.92*	0.22 ± 0.12
BNPs 3.4 μM	83.90 ± 2.55*	14.77 ± 1.53*	0.60 ± 0.44
2 mM H_2O_2	12.73 ± 1.59***	87.03 ± 1.70**	0.23 ± 0.17